APPLICATIONS OF QCD

P.V. Landshoff
Department of Applied Mathematics and Theoretical Physics, University of Cambridge, England.

CONTENTS

1. DEEP INELASTIC LEPTON SCATTERING

The experiments at SLAC in 1969 on deep inelastic lepton scattering mark the beginning of high energy physics as we know it today. They led to the formulation of the parton model and hence to the idea that pointlike quarks are the fundamental hadronic objects to which currents couple, an idea that is central to the structure of modern gauge theories. In this first lecture I am going to remind you about deep inelastic lepton scattering and how it is analysed through the parton model. A more detailed account may be found in, for example, the book by Close[1].

Consider then the set of reactions

$$\ell + N \rightarrow \ell' + X \qquad (1)$$

where ℓ and ℓ' are leptons, N is a target nucleon, and X is a system of hadrons. These reactions are described by the diagram of figure 1, which shows the exchange of a virtual photon, W or Z between the lepton line and the target, so breaking up the target into a set of hadrons X. The main interest is in deep-inelastic events, where the momentum transfer q^2 of the γ, W or Z is large. As we shall see, these events probe the short-distance structure of the target nucleon.

An important feature of the quark parton model is that it relates a number of apparently rather different reactions:

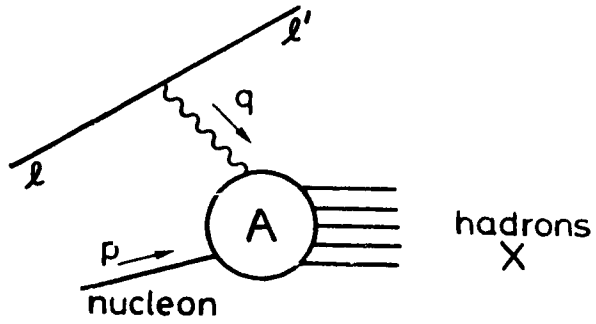

Figure 1 : Deep inelastic lepton scattering through the exchange of a virtual , W or Z.

$$\left.\begin{array}{l} eN \to eX \\ \mu N \to \mu X \end{array}\right\} \ (\gamma \text{ exchange})$$
$$\nu N \to \mu X \quad (W \text{ exchange})$$
$$\nu N \to \nu X \quad (Z \text{ exchange}) \qquad (2)$$

For definiteness, consider either of the two γ-exchange processes. For these, figure 1 corresponds to the expression

$$e\left[\bar{u}(\ell')\ \gamma_\lambda\ u(\ell)\right]\ (g^{\lambda\mu}/q^2)\ A_\mu(\gamma^* N \to X)$$

$$= e\bar{u}(\ell')\ \gamma^\mu\ u(\ell)\ A_\mu/q^2 \qquad (3)$$

Here u and $\bar{u}$ are spinor wave functions for the initial and final leptons, $g^{\lambda\mu}/q^2$ is the photon propagator, and A_μ is an unknown amplitude — it is determined by strong interactions and depends on the structure of the target nucleon.

In most experiments the final-state hadronic system X is not investigated, so to calculate the cross-section we must square the amplitude (3) and sum over X. Notice that in (3) μ is a dummy index of summation, so that when we multiply (3) by its complex conjugate we must introduce a second dummy summation index ν. The interesting part of the product is the factor

$$W_{\mu\nu} = \sum_X A_\mu\ A_\nu^* \qquad (4)$$

$W_{\mu\nu}$ is a function of the target 4-momentum p, the photon 4-momentum q, and the spin vector of the target nucleon. In most experiments the target is unpolarised, so that we must average over its spin states, leaving $W_{\mu\nu}$ a function of p and q only. Because it is a tensor, its structure must therefore be

$$W_{\mu\nu} = -g_{\mu\nu}W_1 + p_\mu p_\nu W_2$$

$$+ \tfrac{1}{2}i\epsilon_{\mu\nu\alpha\beta}q^\alpha p^\beta W_3 + \ldots . \qquad (5)$$

where $W_1, W_2, \ldots$ are functions of the Lorentz scalars q^2 and $\nu = p.q$. [Notice that it is usual to name the coefficient of $g_{\mu\nu}$ as $-W_1$, but some authors write W_2/M^2 instead of W_2, and $\nu = p.q/M$, where M is the target mass.] In the case of γ exchange, parity conservation requires $W_3 = 0$, but W_3 is needed for the W and Z exchange reactions. The terms not written in (5) involve

$$q_\mu p_\nu \ , \quad p_\mu q_\nu \ , \quad q_\mu q_\nu \qquad (6)$$

However, remember that $W_{\mu\nu}$ must be multiplied by a factor coming from the lepton line, and

$$\bar{u}(\ell')\ \gamma.q\ u(\ell) \ = \ \bar{u}(\ell')\gamma\ .\ (k-k')\ u(\ell) \qquad (7)$$

where k and k' are the momenta of the initial and final leptons ℓ and ℓ'. So the Dirac equation implies that the terms (6) give contributions proportional to lepton mass, and so they are negligibly small.

The variable q^2 is a momentum transfer and so it is negative. One commonly defines the two new variables

$$Q^2 = -q^2$$

$$\omega = 2\nu/Q^2 \qquad (8)$$

The dimensionless variable ω is called the Bjorken variable. In the way I have defined them, W_1 and νW_2 are dimensionless functions. It is usual to write

$$W_1(q^2,\nu) = F_1(\omega,Q^2)$$

$$\nu W_2(q^2,\nu) = F_2(\omega,Q^2) \qquad (9)$$

Experiment finds that when Q^2 is large, to a very good approximation F_1 and F_2 depend only on ω and not on Q^2. In the case of the neutrino processes, the same applies to $F_3(\omega,Q^2) = \nu W_3$. This property is known as Bjorken scaling.

This important discovery implies that whatever structure in the nucleon is responsible for absorbing the virtual photon, it is effectively pointlike. For suppose that F_1 and F_2 did vary with Q^2. Then, because

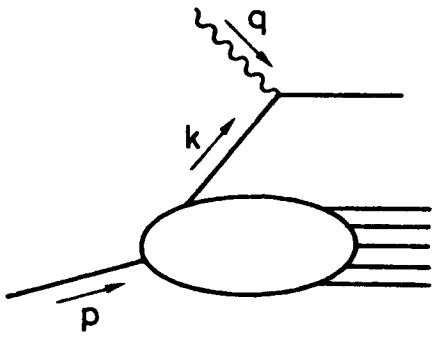

Figure 2 : Absorption of the virtual photon by a quark parton.

they are dimensionless, they must be functions of Q^2/Q_o^2 for some fixed Q_o. Then the cross-section would depend on a fixed length $1/Q_o$.

So Bjorken scaling suggests that the virtual photon couples to pointlike objects in the nucleon. These objects are called partons, and a natural guess is that the partons are quarks. This guess is reinforced by another experimental finding, that to a good approximation

$$F_1(\omega) = \tfrac{1}{2}\omega F_2(\omega) \qquad (10)$$

This is known as the Callan-Gross relation. It may be shown to imply that the virtual photon is transversely polarised and, more important, that the partons have spin ½. Spin 0 partons would give $F_1(\omega) = 0$.

The picture we have, then, is that the virtual photon is absorbed by a quark parton (figure 2). However, this raises a big problem: no quarks have been observed in the final state. The solution to this confinement problem is not understood, but it must be that somehow a final-state interaction prevents fractionally-charged objects from escaping into the final state. Experiment finds that, instead of a quark, there is a jet of hadrons. A jet is a group of particles whose momenta are approximately parallel. Although we do not understand how this comes about, the guess is that it is associated with the chromo-electric field, which is the QCD analogue of the QED electric field. As the quark tries to escape from the vicinity of its parent nucleon, a chromo-electric field is set up between it and the remaining nucleon fragments. It is simple to show that, if for some unknown reason this field is confined to a tube instead of spreading out in all directions, its energy increases as the quark gets further away. This energy is provided by the slowing down of the quark. When the field energy is high enough, it can create new quark-antiquark pairs. The antiquark fuses with the original quark to form a meson, and the new quark tries to escape. The process is then repeated, so that further mesons are created and form a jet. Thus figure 2 becomes figure 3a. The particle momenta in the γN centre-of-mass frame are drawn in figure 3b, which shows

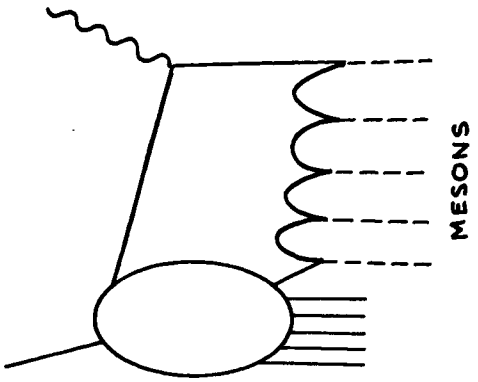

(a)

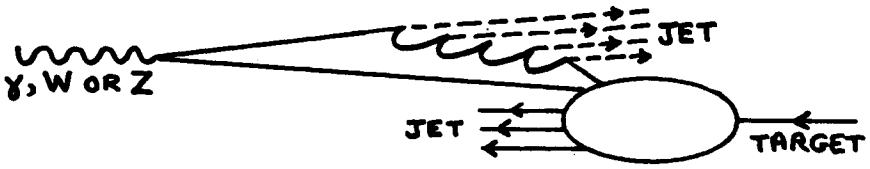

(b)

Figure 3 : Jet creation : (a) the effect on figure 2 of final-state interaction; (b) particle momenta in the γN centre-of-mass frame.

also the jet associated with the residual nucleon fragments.

The key assumption in the calculation[1,2] of the structure functions F_1, F_2 and F_3 in the parton model is that, in a frame where the nucleon 3-momentum $|\underset{\sim}{p}|$ is large, the 4-momentum of the constituent partons is almost parallel to p :

$$k \approx xp \tag{11}$$

This amounts to saying that in the nucleon rest frame the partons do not have large momentum. One introduces an x distribution for each parton flavour:

$$q(x)dx = \text{the expectation value of the number of partons of flavour q with x in the range } (x, x+dx) \quad (q = u,d,s,c,b \ldots) \tag{12}$$

One also uses the charge symmetry of the strong interactions, so that for example the u-distribution in the proton is the same as the d-distribution in the neutron. Finally, one uses the couplings of the γ, W and Z to leptons and quarks that are given by the Salam-Weinberg model (see Peccei's lectures).

An important result that derives from the kinematics of the parton model is that

$$x = 1/\omega \tag{13}$$

According to (8), ω is measured from the momenta of the initial and final leptons, so this result says that by seeing how the lepton is scattered we deduce the fractional momentum x of the quark that is responsible for the scattering. The various reactions (2) are all calculable in terms of the quark distributions q(x), for example

$$F_2^{\mu p}(\omega,Q^2) = \frac{4}{9}\left[x\,u(x) + x\,\bar{u}(x)\right] + \frac{1}{9}\left[xd + x\bar{d} + xs + x\bar{s}\right] \tag{14}$$

with contributions from the heavier quarks switching on at larger values of Q^2.

It is of course not trivial that the various reactions μp, μn, νp, $\bar{\nu} p$, νn, $\bar{\nu} n$ can all be calculated in terms of the same functions u(x), d(x),... . That this works well is an important rest of the quark parton model. For example, figure 4 shows one such test, the Gross-Llewellyn Sum Rule. This predicts that

$$\tfrac{1}{2}\int_1^\infty \frac{d\omega}{\omega^2}\,(F_3^{\nu p} + F_3^{\nu n}) = -3 \tag{15}$$

Another, more detailed, test is that for each value of ω

$$6\omega\,(F_2^{\mu p} - F_2^{\mu n}) = F_3^{\nu p} - F_3^{\nu n} \tag{16}$$

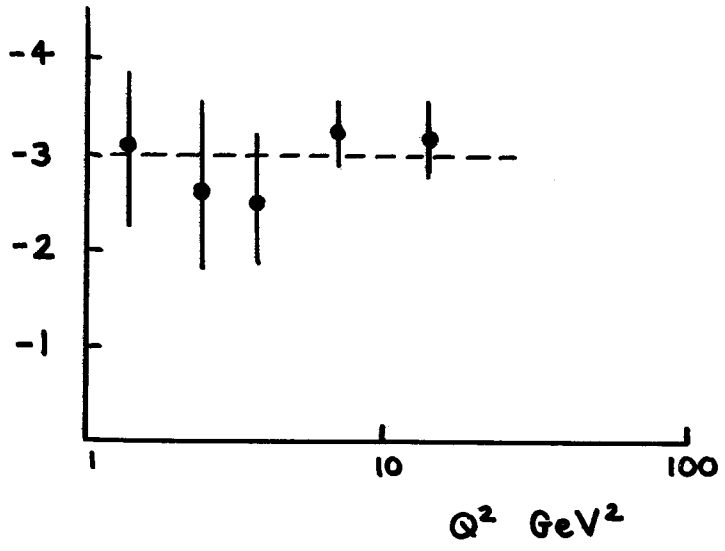

Figure 4 : Test of the Gross-Llewellyn Smith sum rule (ABCLOS collaboration).

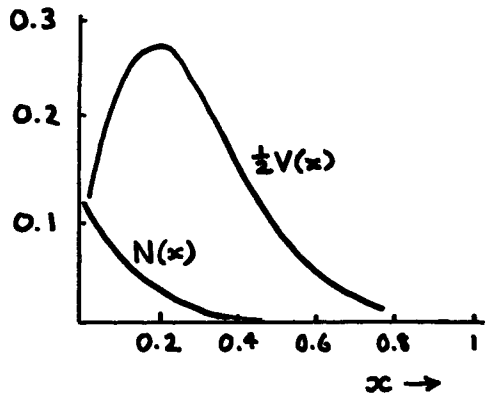

Figure 5 : Sketches of the distributions of valence and non-valence quarks in the nucleon.

By combining data from the various reactions, one may extract the separate parton densities u(x), d(x) .... The resulting picture of the nucleon is a little more complicated than the original three-quark structure postulated by Gell-Mann and Zweig. Instead

$$\text{proton} = (uud) + \begin{array}{l}\text{neutral "sea" of}\\ q\bar{q}\text{ pairs and}\\ \text{gluons}\end{array} \qquad (17)$$

The (uud) are called valence quarks and give the proton its quantum numbers, while the sea is neutral and is the same for proton and neutron. It seems to be valid to regard each parton distribution as a sum of valence and non-valence parts, though strictly one might expect some quantum-mechanical interference between the two. Thus

$$\begin{aligned} x\,u(x) &= V(x) + N(x) \\ x\,\bar{u}(x) &= \qquad N(x) \end{aligned} \qquad (18)$$

where N(x) is the non-valence part. Experiment seems to find[3] that the sea is SU(2) invariant, so that the d-quarks have the same non-valence distribution. The simplest assumption is that their valence distribution is again proportional to V(x), but with a factor ½ because there are half as many valence d quarks in the proton as valence u quarks:

$$\begin{aligned} x\,d(x) &= \tfrac{1}{2}V(x) + N(x) \\ x\,\bar{d}(x) &= \qquad N(x) \end{aligned} \qquad (19)$$

This assumption works well enough as a first approximation, though it is not exact because it is now well established[3] that actually the d-quark distribution falls off more rapidly than the u-quark distribution as $x \to 1$. The distributions of the heavier quarks are entirely non-valence. Their shapes seem[3] to be the same as that of $N(x)$, but their normalisations are probably rather smaller, even when Q^2 is large enough for them to be fully "switched on".

In figure 5 I sketch the valence and non-valence distributions. Notice that $N(x)$ is very small except at small values of x. The behaviour of the two functions as $x \to 0$ is controlled by Regge theory[2] : $N(x) \to$ constant, corresponding to pomeron exchange, while

$$V(x) \sim x^{1-\alpha(o)} \tag{20}$$

where $\alpha(o)$ is the intercept of the exchange-degenerate (ρ,ω,f,A_2) trajectory, with $\alpha(o) \approx \frac{1}{2}$. So for very small x,

$$q(x) \approx \frac{1}{x} N(x) \tag{21}$$

for $q = u,d,\bar{u},\bar{d} \ldots$. Hence the number of partons of each flavour with fractional momentum less than ϵ,

$$\int_0^\epsilon dx\, q(x) \ , \tag{22}$$

diverges logarithmically. That is, the sea contains a very large number of very-small-x partons.

Finally, one may calculate the total fractional momentum carried by all the quarks and antiquarks:

$$\int_0^1 dx\, x\left[u(x) + \bar{u}(x) + d(x) + \ldots\right] \tag{23}$$

Experiment finds a value near to $\frac{1}{2}$. The other half of the momentum of the target must be carried by objects to which the γ, W and Z do not couple. It is commonly assumed that these are just the gluons of QCD.

2. OTHER PARTON PHYSICS

The Drell-Yan Process

Figure 6, which is reproduced from the front cover of the booklet for the 1978 CERN School, shows data for the process

$$p+N \to \mu^+\mu^- + X \tag{24}$$

The cross section is plotted against the invariant mass $m_{\mu\mu}$ of the muon

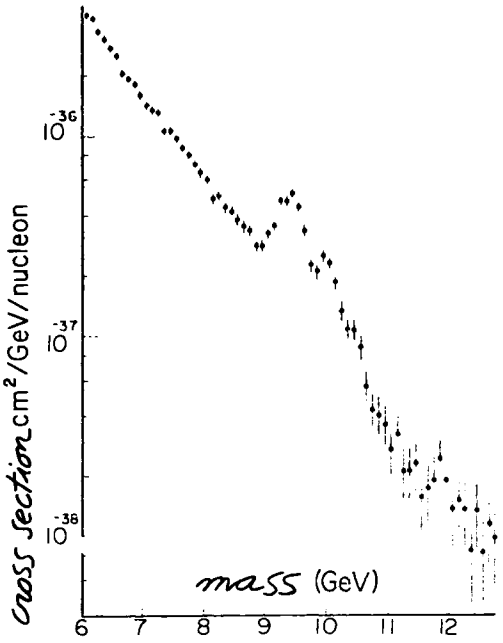

Figure 6 : Data for pN → $\mu^+\mu^-$ + X (CFS collaboration).

pair, and shows the Υ, Υ' and Υ'' resonances. My concern here is with the non-resonant background continuum, which for large values of $m_{\mu\mu}$ (such as are represented in the data of figure 6) is described by the Drell-Yan quark-antiquark fusion mechanism of figure 7. I have not shown in figure 7 possible additional final-state interactions between the two jets of hadrons. Certainly these are needed to achieve confinement, as I discussed for the case of deep inelastic scattering. There is at present some controversy as to whether they have any substantial effect on the cross-section. My guess is that it will eventually be agreed that, somewhat

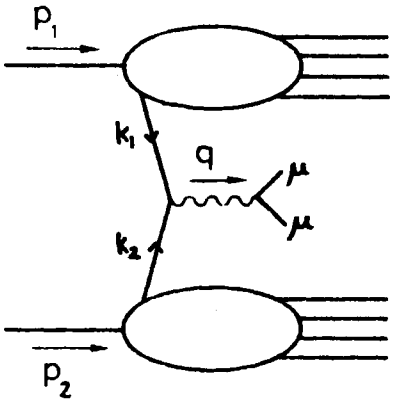

Figure 7 : The Drell-Yan mechanism.

miraculously, they do not change the value of the inclusive cross section for the case when only the final-state muons, and not the hadrons, are detected. Some of the relevant papers are those of reference 4.

It will be seen that the amplitudes at the top and bottom of figure 7 are the same as the amplitude that occurs in the deep inelastic scattering diagram of figure 2. So the Drell-Yan process may be calculated in terms of the same parton distributions $u(x)$, $\bar{u}(x)$, $d(x)$ ... that occur in deep inelastic scattering. This close connection between two very different sorts of reaction is all the more remarkable in that the Drell-Yan process involves a timelike photon, with $q^2 = m_{\mu\mu}^2 > 0$, while in deep inelastic scattering $q^2 < 0$.

According to equation (11), in a frame where a hadron is moving fast its constituent partons move almost parallel to it. So we have

$$k_1 \approx x_1 p_1 \qquad k_2 \approx x_2 p_2 \tag{25}$$

So $q^2 = (k_1+k_2)^2 = (x_1p_1+x_2p_2)^2 \approx 2x_1x_2 p_1.p_2$, or

$$x_1 x_2 \approx \tau \tag{26}$$

where $\tau = q^2/s$, with $s = (p_1+p_2)^2 \approx 2p_1.p_2$. In the centre-of-mass frame

$$p_1 \approx (\tfrac{1}{2}\sqrt{s},0,0,\tfrac{1}{2}\sqrt{s}) \ , \quad p_2 = (\tfrac{1}{2}\sqrt{s},0,0,-\tfrac{1}{2}\sqrt{s}) \tag{27}$$

and so the longitudinal component of q is $q_L = (x_1p_1+x_2p_2)_z = \tfrac{1}{2}\sqrt{s}(x_1-x_2)$. Thus

$$x_1 - x_2 = x_F \tag{28}$$

where x_F is the Feynman variable, $x_F = q_L/\tfrac{1}{2}\sqrt{s}$. Thus x_1 and x_2 may be found by measuring x_F and τ, and then solving the simultaneous equations (26) and (28). So, as in deep inelastic scattering, the parton fractional momentum x may be found by measuring the lepton momenta.

Calculation gives[1]

$$\frac{d^2\sigma}{dx_F d\tau} = \frac{1}{3} \frac{4\pi\alpha^2}{3m_{\mu\mu}^2} \frac{1}{x_1+x_2} F(x_1,x_2) \tag{29}$$

with

$$F(x_1,x_2) = \frac{4}{9} u(x_1)\ \bar{u}(x_2) + \frac{1}{9} d(x_1)\ \bar{d}(x_2) + (x_1 \leftrightarrow x_2) + \ldots \tag{30}$$

where I have not written contributions from heavier quarks. The factor $\frac{1}{3}$ in (29) is present because of colour: the quark and antiquark can only

fuse to form a photon if their colours are equal and opposite, and there is a 1 in 3 chance of this being true.

Taking the parton distributions from deep inelastic scattering, one can calculate (29) completely. The agreement with experiment is extremely good, provided one introduces an additional multiplicative factor

$$K \approx 2.2 \tag{31}$$

This K-factor is believed to originate in QCD corrections to the Drell-Yan mechanism. I shall explain this further in §3.

The Drell-Yan process is important for a number of reasons. Not only is it a non-trivial test of the parton model, it also enables one to measure structure functions for hadrons other than nucleons. For example, the structure functions F_2 of the pion cannot be measured in deep inelastic scattering because pion targets are not possible, but measuring the Drell-Yan process with a pion beam gives the same information. The result is shown in figure 8: the structure function of the pion is found to fall off rather more slowly as $x \to 1$ than does that of the nucleon.

Another, very important, feature of the Drell-Yan mechanism is that it allows W and Z production in hadronic collisions — in figure 7 the virtual photon is replaced by the W or Z. The predicted cross-sections for the CERN $\bar{p}p$ collider are at the nanobarn level.

e^+e^- Annihilation

To lowest order in the electromagnetic coupling α, the process

$$e^+e^- \to \mu^+\mu^- \tag{32}$$

is calculated from the single diagram of figure 9. The result is

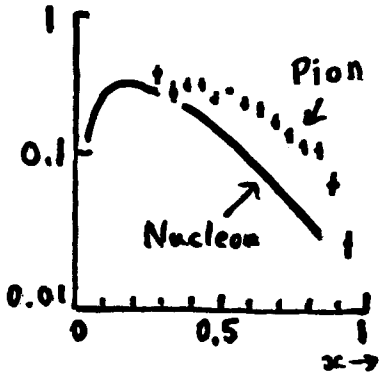

Figure 8 : Measurements of the structure function F_2 of the pion from the Drell-Yan process (CIP collaboration).

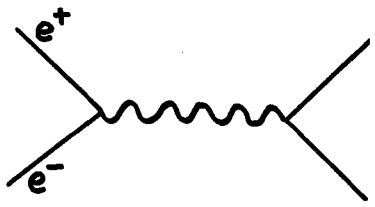

Figure 9 : Diagram for $e^+e^- \to \mu^+\mu^-$ or $e^+e^- \to q\bar{q}$.

$$\frac{d\sigma}{d(\cos\theta)} = \frac{\pi\alpha^2}{2s}(1 + \cos^2\theta) \tag{33}$$

where $\sqrt{s}$ is the centre-of-mass energy and θ the angle at which the μ^+ emerges relative to the e^+. If one replaces the muon line in figure 9 by a quark line, one obtains a possible mechanism for the process

$$e^+e^- \to \text{hadrons} \tag{34}$$

The only difference in the calculation of the new diagram is that the quark has fractional charge e_i instead of integral charge e, so one has

$$R = \frac{\sigma(e^+e^- \to \text{hadrons})}{\sigma(e^+e^- \to \mu^+\mu^-)} = 3 \sum_{i=u,d,\ldots} (e_i/e)^2 \tag{35}$$

The factor 3 here enters because each flavour i of the quark can be produced in 3 versions of different colours. Data for R are shown in figure 10; for $\sqrt{s}$ between 12 and 36 GeV they fit very well to the

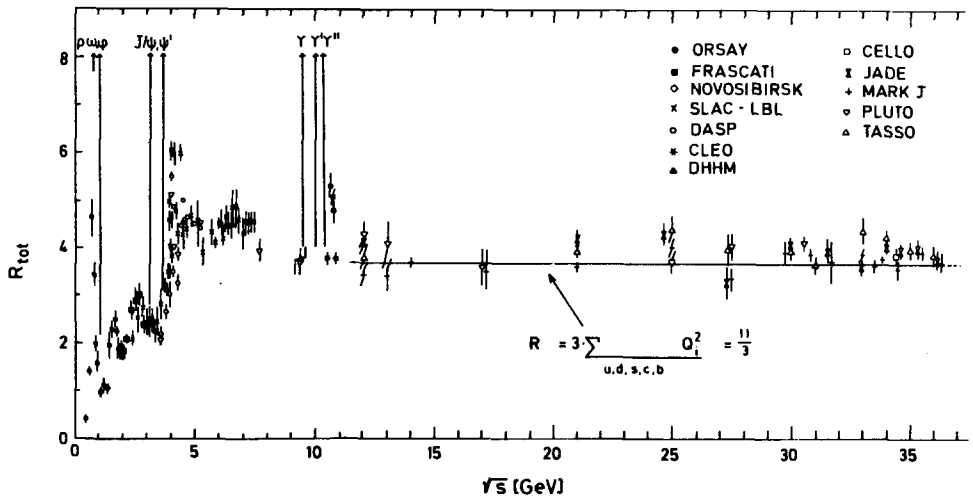

Figure 10 : Data for $R_{e^+e^-}$.

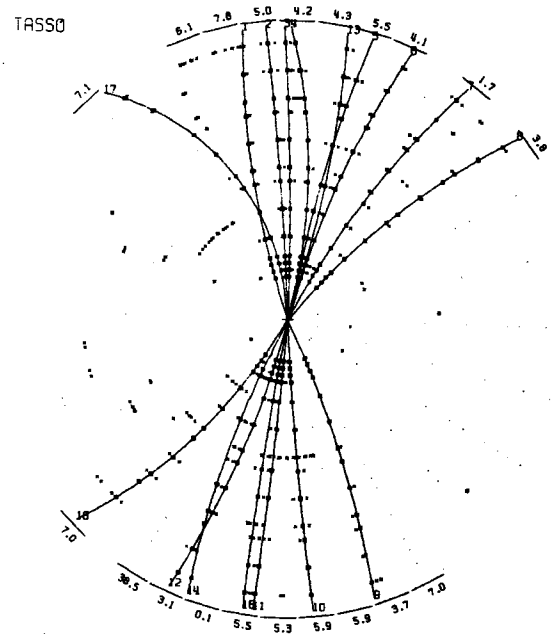

Figure 11 : A typical two-jet event in e^+e^- annihilation.

expression (35), with i = u,d,s,c,b included. It is evident that there is no room in the data for the inclusion of a t quark, which would increase R by 12/9. Notice that these data are the best evidence for the need for three colours.

Just as I explained in §1, the q and $\bar{q}$ are not seen in the final state: instead, one sees a pair of jets. Because the experiments are performed with the e^+ and e^- colliding head-on, the two jets emerge back-to-back. A typical event is seen in figure 11.

Some evidence that the two jets are indeed associated with quarks comes from the angular distribution of the jet axis (the direction of the total momentum of the particles in a jet) relative to the beam direction. As the quarks have spin ½ this angular distribution should be $1+\cos^2\theta$ as in (33), and this is what is found. Spin 0 partons would instead give $\sin^2\theta$, which does not agree with experiment.

One may investigate whether the jets have the same structure as the forward jet in deep inelastic scattering (see figure 3). One distribution that is important is the jet fragmentation function. The jet axis is identified and the component p_L of the momentum of each hadron along the jet axis is measured. Define

$$z = p_L/E^{Jet} \tag{36}$$

where E^{Jet} is the total energy of the jet. It is then found that, for each type of hadron, the distribution dN/dz satisfies an approximate scaling law:

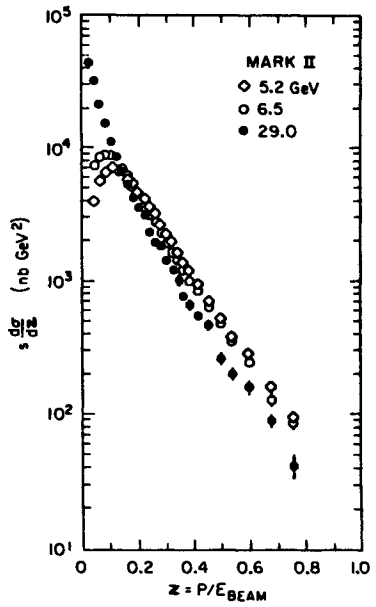

Figure 12 : Data for the jet fragmentation function dN/dz.

to a first approximation it is a function of z only, independent of p^{Jet}. See figure 12. This scaling is theoretically related[2] to Bjorken scaling in deep inelastic scattering. Just as in deep inelastic scattering, nowadays the interest is not so much in how well it is satisfied, but more in how much it is violated. Very similar jet fragmentation functions are measured in deep inelastic scattering, in experiments that look at the final-state hadrons.

Photon-Photon Collisions

Figure 13 shows the lowest-order diagram for the process

$$e^+e^- \rightarrow e^+e^-\mu^+\mu^- \qquad (37)$$

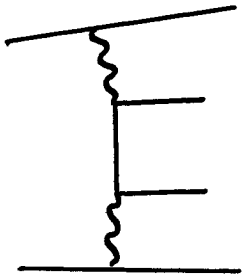

Figure 13 : Diagram for $e^+e^- \rightarrow e^+e^-\mu^+\mu^-$ or $e^+e^- \rightarrow e^+e^-q\bar{q}$.

It gives a cross-section proportional to α^4, compared with α^2 for the annihilation process (32). Nevertheless, the "$\gamma\gamma$ process" (37) has a much larger cross-section. This is because the kinematics allow th momentum transfers q_1^2 and q_2^2 carried by the two internal virtual photons to be close to 0, and the more so as the total centre-of-mass energy $\sqrt{s}$ increases. So the integration over the final-state momenta needed to calculate the cross-section receives large contributions from the photon propagators (which are, of course, proportional to $1/q_1^2$ and $1/q_2^2$). The result is a cross-section that rises logarithmically with $\sqrt{s}$, while according to (33) the annihilation cross-section falls like $1/s$. At $\sqrt{s}$ = 100 GeV, the cross-section for the $\gamma\gamma$ process (37) is more than 4 orders of magnitude greater than that for the annihilation process (32).

Unfortunately, most of the $\gamma\gamma$ events are very hard to detect as the final-state particles tend to go down the beam pipes. Nevertheless, interesting physics can be done. For a recent review see reference 5.

As an example, suppose that the muon line in figure 13 is replaced by a quark line. This results in the $\gamma\gamma$ process

$$e^+e^- \rightarrow e^+e^- + \text{hadrons} \qquad (38)$$

with the hadrons emerging in two jets whose structure should be identical with those in the annihilation process (34). In general, the virtual photons have different momenta, so in the $\gamma\gamma$ process the jets are not

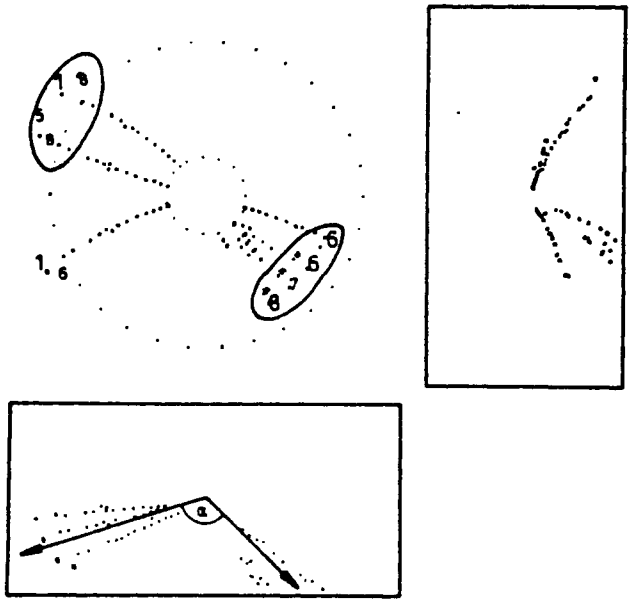

Figure 14 : A two-jet event in a $\gamma\gamma$ process; three orthogonal views are shown (PLUTO).

expected to be back-to-back. An event is shown in figure 14, which shows this clearly.

3. QCD PHENOMENOLOGY

So far I have reviewed, very quickly, the applications of the simple parton model. I now consider how the parton model is modified by QCD effects. In this section, the discussion is qualitative and assumes very little detailed knowledge of QCD.

I am going to review just a few of the many qualitative successes of QCD. More complete reviews may be found in the papers of reference 6 and in Barbiellini's lectures. As I shall explain, the successes are qualitative rather than quantitative, because we do not know how to perform precise calculations. There are two main difficulties, the presence of uncalculable higher twist effects, which I mention in this section, and the problem of substantial renormalisation-scheme dependence of calculations, dealt with in §5.

Jet Widening in e^+e^- Annihilation

I have explained that the simple parton model predicts that in high-energy e^+e^- annihilation into hadrons the final state should consist of

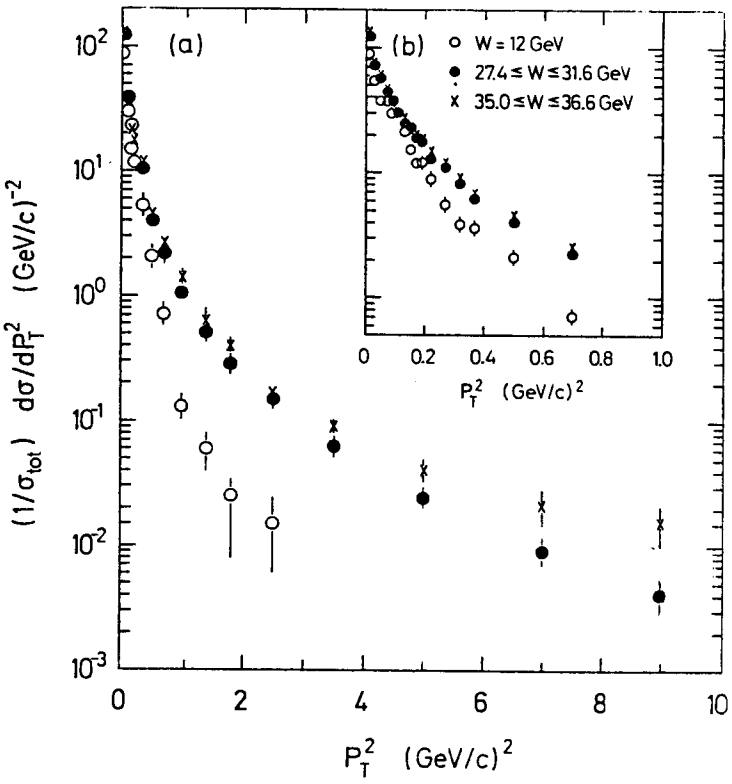

Figure 15 : p_T distribution relative to the jet axis in e^+e^- annihilation (PLUTO).

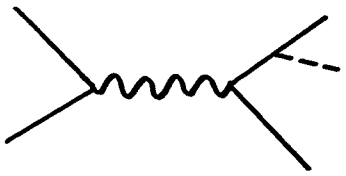

Figure 16 : Gluon radiation from a quark (or antiquark) in e^+e^- annihilation.

two jets. Suppose that this is assumed to be true, and that the jet axis has been found. One way to do this is to guess a direction for the axis, measure the transverse momentum p_T of each particle relative to this direction, and then vary the direction so as to minimise Σp_T^2. Figure 15 shows the p_T distribution relative to the resulting jet axis, which is seen to become wider as the centre-of-mass energy increases.

This jet widening is attributed to gluon radiation: one of the quarks in figure 9 radiates a gluon, as is shown in figure 16. In most events of this type, the gluon emerges almost in the same direction as that of the quark with which it is associated, so resulting in a two-jet event with one jet slightly widened. Sometimes, however, the gluon comes out in a different direction from the quark. Gluons, like quarks, seem to be subject to a confinement law and are not detected as such; what is seen in these events are three jets of ordinary hadrons. An example is shown in figure 17.

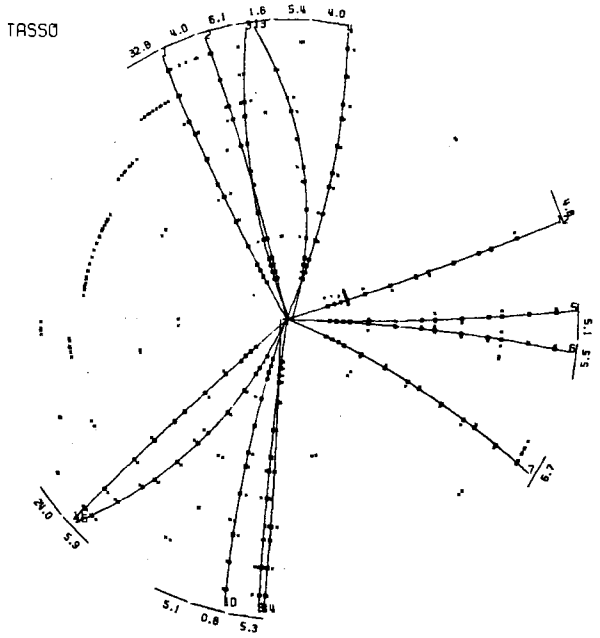

Figure 17 : A three-jet event in e^+e^- annihilation.

One may calculate from figure 16 the cross-section for producing three-jet events, and the angular distributions of the jets. Agreement with experiment is very encouraging. However, it is worth emphasising that one has no right to expect perfect agreement, for a number of reasons. First, there are the difficulties with the perturbation-theory calculation, which I discuss at the end of these lectures. Equally important, there are the very real uncertainties that arise from the fact that only part of the calculation is based on QCD perturbation theory. The way in which the quarks and gluons fragment into hadrons cannot be calculated, but must be taken from experiment. A given quark will fragment in a different way from event to event, that is information such as the fragmentation function shown in figure 12 is averaged over many events. Fluctuations from the average are very important for calculations of 3-jet events; for example, just occasionally a fluctuation in the hadronisation of one of the quarks in an event that really originates from figure 9 can make it appear to be a 3-jet event. Thus data have to be analysed using Monte Carlo calculations that contain detailed models of how the quarks and gluons hadronise. Notice that similar detailed Monte Carlo calculations are needed not just to calculate the theory, but also to correct the data for the limited acceptance of the detectors. There are different detailed models of the jet hadronisation and one might expect that, with this rather tortuous procedure, they might lead to rather different output conclusions. Whether or not this is so is at present controversial[7].

Scale-Breaking in Deep Inelastic Lepton Scattering

In the presence of QCD corrections, the simple parton model of figure 2 is regarded as the zeroth-order term in a perturbation expansion in powers of the QCD coupling α_s. I remind you that the top part of the diagram is calculated from QED perturbation theory, but the bottom part of the diagram cannot be calculated from perturbation theory and must be taken from experiment.

The $0(\alpha_s)$ terms in the perturbation expansion are drawn in figure 18 (there is also a virtual-gluon correction to figure 2, which I have not

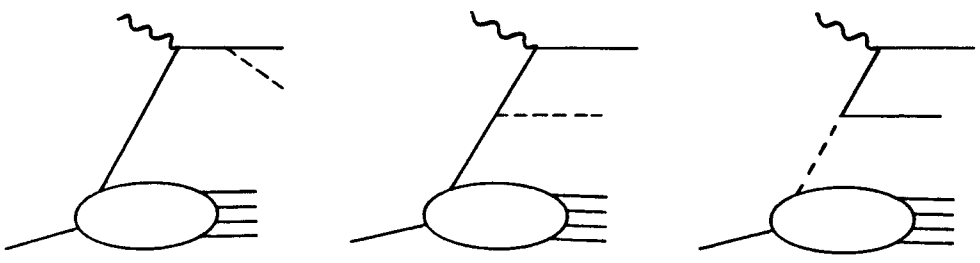

Figure 18 : $0(\alpha_s)$ terms in deep inelastic scattering.

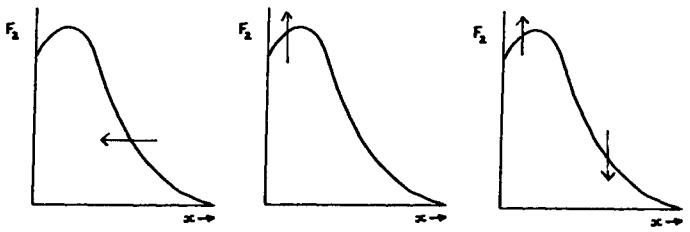

Figure 19 : Variation of F_2 as Q^2 increases: (a) from figure 18b, (b) from figure 18c, (c) combined effect.

shown). In each case, the bottom bubble is not calculable and must be taken from experiment, because it involves long-distance strong interactions. The upper parts of the diagrams involve a short-distance interaction, so that the appropriate running coupling α_s is small and they may be calculated by a combination of QCD and QED perturbation theory. In figures 18a and 18b the bottom bubbles are just the quark distributions u(x), d(x) .... of §1, but figure 18c involves a new function, the gluon distribution in the target nucleon.

The physical interpretation of the different diagrams of figure 18 is gauge-dependent, and is simplest in certain axial gauges. In these gauges, figure 18a corresponds to a widening of the forward jet, just like in e^+e^- annihilation. In a small fraction of the events, it yields two separate forward jets. In figure 18b, the gluon carries away some of the fractional momentum of the quark, so that the x-value probed by the virtual photon is less than that of the original parton. It turns out that this effect becomes more important with increasing Q^2, so that it makes the plot of F_2 against $1/\omega$ move to the left as Q^2 increases (figure 19a). Figure 18c generates additional $q\bar{q}$ pairs as Q^2 increases,

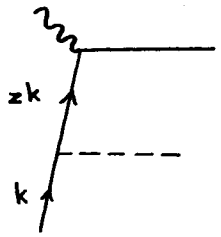

Figure 20 : Diagram for the Altarelli-Parisi kernel $P_{q \leftarrow q}(z)$.

so that the contribution to F_2 from the sea increases. As the sea-contribution is mainly confined to small $1/\omega$ (see figure 5), the effect on F_2 is a rise at small $1/\omega$ as shown in figure 19b. The combined effect on F_2 is as shown in figure 19c.

All this is made quantitative in the Altarelli-Parisi evolution equation. I shall describe roughly how this equation is derived; for a more complete account see reference 8. Figure 20 shows the upper part of figure 18b. One uses it to calculate from perturbation theory a function

$$\frac{\alpha_s}{2\pi} \; P_{q \leftarrow q}(z) \tag{39}$$

This function is called the "Altarelli-Parisi kernel", or sometimes the "splitting function". It is associated with the probability that the virtual photon is absorbed by a quark that has a fraction z of the momentum of the original quark. (One needs also the virtual-gluon term to calculate it.) It is used to calculate the variation of $F_2(\omega,Q^2)$ with Q^2 :

$$Q^2 \frac{dF_2(\omega,Q^2)}{dQ^2} = \frac{\alpha_s}{2\pi} \int dy\, dz \;\; F_2(\tfrac{1}{y},Q^2) P_{q \leftarrow q}(z) \;\; \delta(yz - \tfrac{1}{\omega}) \tag{40}$$

Let us try to get some understanding of the terms in this equation. It is the logarithmic derivative $Q^2 d/dQ^2$ that appears on the left-hand side, so as to keep it dimensionless. On the right-hand side, y is the fractional momentum of the quark that originally emerges from the target, $k = yp$. Because the Altarelli-Parisi kernel (39) is already of order α_s, to calculate the $0(\alpha_s)$ contribution to the derivative of F_2 we need only the zeroth-order contribution to F_2 on the right-hand side. According to (13), y^{-1} is just the Bjorken variable for this zeroth-order term. In figure 20, the final quark momentum is $(zk+q)$. If we insert $k = yp$ and use the definition (8) of the Bjorken variable as measured from the momenta of the initial and final leptons, the condition that this quark be "on shell" gives the δ-function in (40). Finally, we have to integrate over all possible values of y and z.

Because of the δ-function, the z integration is trivial. Figure 18c results in an additional term on the right-hand side, so that altogether

$$Q^2 \frac{dF_2}{dQ^2} = \frac{\alpha_s}{2\pi} \int_{1/\omega}^{1} \frac{dy}{y} \left[F_2(\tfrac{1}{y},Q^2) \;\; P_{q \leftarrow q} \;\; (\tfrac{1}{y\omega}) \right.$$

$$\left. + \; G(\tfrac{1}{y},Q^2) \;\; P_{q \leftarrow g} \;\; (\tfrac{1}{y\omega}) \right] \tag{41}$$

Here, $P_{q \leftarrow g}$ is calculated from the upper part of figure 18c, and the

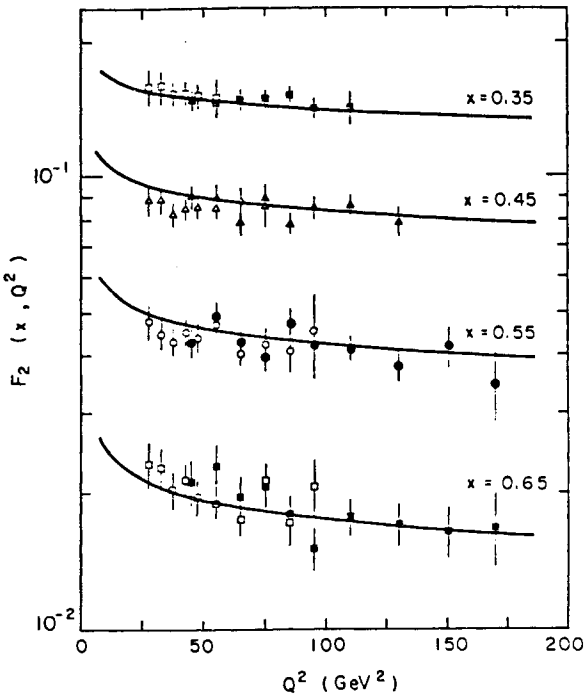

Figure 21 : Data for F_2 from the scattering of muons on carbon, together with QCD calculations (BCDMS collaboration).

function G is the uncalculable lower part. Data analyses often eliminate the gluon term by considering "non-singlet" structure functions, that is either the combination $(F_2^{\mu p} - F_2^{\mu n})$ where all non-valence contributions cancel between the two terms, or F_3 in neutrino processes, where it may be shown that non-valence contributions do not occur either.

A typical data analysis is shown in figure 21, from which it is concluded that the QCD scale parameter Λ = 85 MeV. Different analyses[3], sometimes even of the same data, tend to produce rather different values of Λ. A big problem is that of higher twists. The equation (41) that results from perturbative QCD gives breaking of Bjorken scaling that is logarithmic in Q^2. The higher twists are inverse powers of Q^2, which cannot be calculated and must be relatively negligible when Q^2 is large enough, but may perhaps be very important in present-day data. Whether or not this is so is controversial. One might hope to extract their magnitude from experiment, but they can be parametrised in different ways, with widely different results. The European Muon Collaboration find that a very good fit to their data, combined with that from SLAC, may be obtained by multiplying the right-hand side of (41) by the factor

$$1 + \frac{m_o^2}{Q^2} \left(\frac{1}{\omega} - 1\right)^{-2} \qquad (42)$$

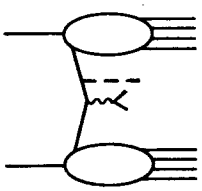

Figure 22 : Gluon radiation in the Drell-Yan process.

with $m_o \approx 700$ MeV. The second term here is the higher twist, and it accounts for a very substantial part of the scale breaking observed for the Q^2 values in the SLAC range. Notice that the value found for m_o is roughly what one expects for a non-perturbative strong interaction effect.

Gluon effects in the Drell-Yan process

In the Drell-Yan diagram of figure 7, the parton momenta k_1 and k_2 are supposed to have small transverse components relative to p_1 and p_2. So $q_T = (k_{1T} + k_{2T})$ is small, at most a few hundred MeV/c in magnitude. However, large values of q_T may be obtained by modifying figure 7 to allow for gluon radiation (figure 22). Here, a large transverse momentum q_T of the dilepton may be balanced by a gluon jet with the opposite transverse momentum. The central part of the diagram is calculated from perturbation theory, while the upper and lower bubbles must, as always, be taken from experiment.

Calculations of q_T distributions from figure 22 can be made to agree well with experiment, but they contain some rather arbitrary ingredients[9]. First, as I shall discuss in §5, there is uncertainty about what one should choose for the argument of the running coupling α_s in the calculation — should it be $m^2_{\mu\mu}$, q^2_T or what? More important, though, is the problem of how to handle the "intrinsic transverse momentum" of the partons in the calculations. This is the transverse momentum that I referred to in the previous paragraph: it is the transverse momentum that the partons have before they interact to produce the virtual photon and the gluon, by virtue of the fact that they are bound constituents of their parent hadrons. It is necessary to incorporate this transverse momentum into the calculation in order to obtain agreement with experiment, but there is no good theoretical understanding of what should be taken for the intrinsic transverse momentum distribution, nor of exactly how to fold it into the QCD perturbation theory calculation.

In spite of the difficulties in making precise calculations, there is good qualitative agreement between theory and experiment. One prediction is that the average q_T should rise with the beam energy, and figure 23 shows that this is well confirmed.

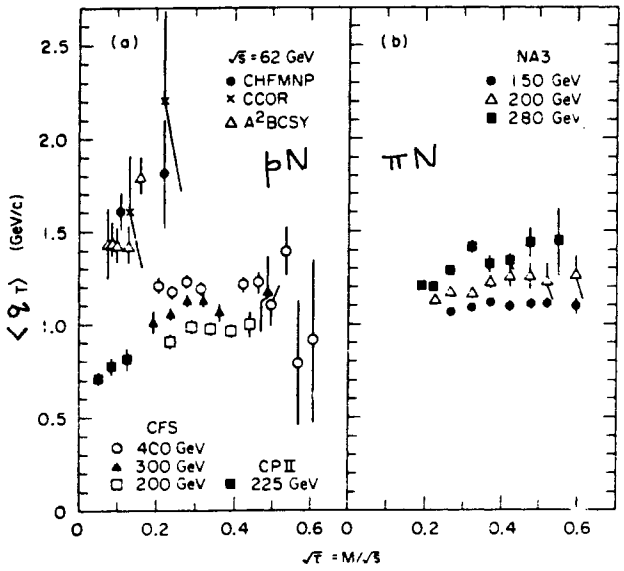

Figure 23 : Average transverse momentum of dileptons.

The K-Factor

I explained in §2 that, in order to obtain agreement with experiment, the Drell-Yan formula (29) must be multiplied by a factor $K \approx 2.2$. This factor is believed to originate from QCD corrections to figure 7.

The theory of this is complicated and is not yet fully worked out. In the Feynman gauge, the most important diagram is that of figure 24, where a virtual gluon is exchanged between the fusing quark and antiquark. Part of the contribution from this diagram is cancelled by other diagrams in which a gluon is radiated, for example figure 23. The most important part of what remains is just a constant factor $\frac{\alpha_s}{\pi} \cdot \frac{8}{9}\pi^2$ that multiplies the uncorrected Drell-Yan diagram. Thus if we add together figure 7 and figure 24, we obtain the correction factor

$$1 + \frac{\alpha_s}{\pi} \frac{8}{9} \pi^2 \qquad (43)$$

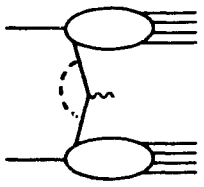

Figure 24 : A QCD correction to the Drell-Yan mechanism.

to the original Drell-Yan formula. It is believed that (43) is the beginning of an exponential series, with the higher powers of α_s coming from multigluon corrections to figure 7. If this is correct, we have

$$K = \exp\left(\frac{\alpha_s}{\pi} \cdot \frac{8}{9}\pi^2\right) \tag{44}$$

In order to get $K \approx 2.2$, we need $\alpha_s \approx 1/4$.

This is a very simplified description of what is a very complicated story. For more details, see the papers of reference 10.

Large p_T Hadronic Processes

Consider the reaction

$$pp \rightarrow \pi + X \tag{45}$$

where, as usual, X denotes a system of hadrons that is not detected. For definiteness, suppose that the detected pion emerges at 90^o in the centre-of-mass frame, so that its momentum p_T is purely transverse.

Events in which p_T is small almost surely arise from peripheral collisions, that is those in which only the outer edges of the two colliding protons interact. Because there is no short-distance interaction, the appropriate running coupling α_s is not small and one cannot calculate with perturbation theory. In order to be able to use perturbation theory, we need a head-on collision, so that a short-distance interaction occurs. There is no certain way of separating off such (rather rare) events, but intuition suggests that a large-p_T final-state particle should be a good indication of them.

Certainly, experiment does seem to confirm that the dynamics of large-p_T events are different from those of small-p_T events. At small p_T, one finds that for 90^o pion production the Lorentz invariant inclusive distribution

$$E\frac{d\sigma}{d^3p} \propto e^{-Cp_T} \tag{46}$$

with $C \approx 6(\text{GeV}/c)^{-1}$. It was discovered a decade ago at the CERN ISR that, for $p_T \gtrsim 1$ GeV/c, the fall-off of $Ed\sigma/d^3p$ as p_T increases is much slower than exponential: some early data are shown in figure 25.

In order to describe large-p_T data, it is usual to introduce the dimensionless variable

$$x_T = 2p_T/\sqrt{s} \tag{47}$$

One may parametrise the data in the form

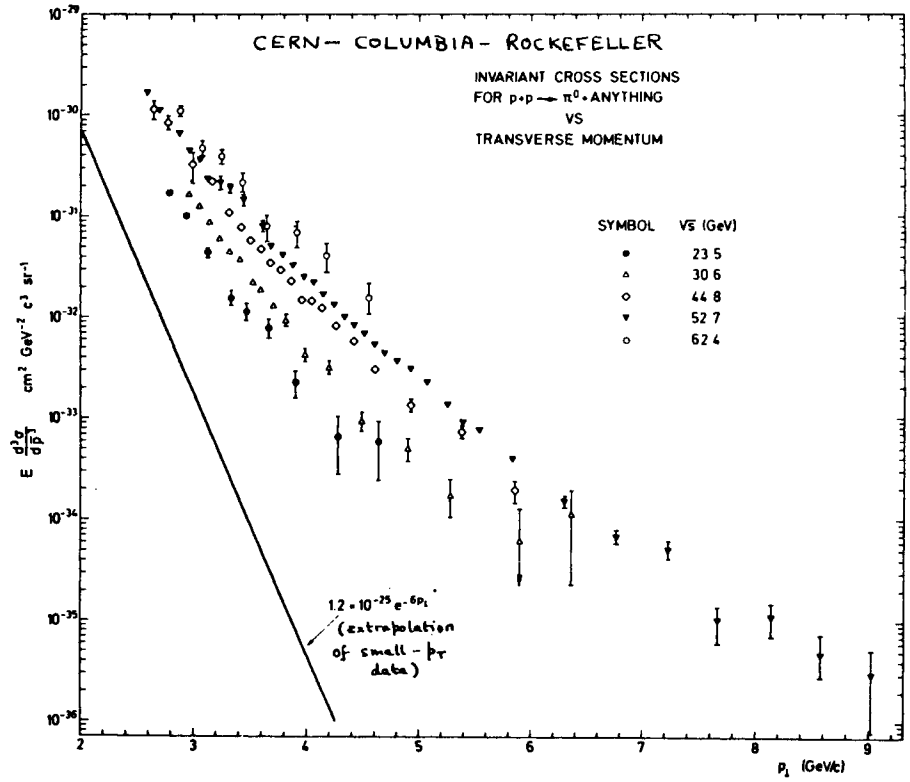

Figure 25 : π^0 production at 90^0 at the CERN ISR. The straight line is an extrapolation of data at small p_T (CCR collaboration).

$$E \frac{d\sigma}{d^3p} = p_T^{-n} F(x_T) \qquad (48)$$

where n can be a function of x_T and $\sqrt{s}$. Suppose, however, that as in deep inelastic scattering and in the Drell-Yan process, the dynamics are scale-free, that is no fixed mass or length appears in the function F. Then F must be dimensionless, and in order that the left-hand side of (48) may have the correct dimensions we must have n = 4.

The ISR data do find that n is a constant to a good approximation, but n = 8 rather than 4. This is shown in figure 26: when plotted against x_T, it is $p_T^8 \, Ed\sigma/d^3p$ that yields a single curve, independent of $\sqrt{s}$. Although explanations for this value of n have been given, I think that it is true to say that there is no single model that gives a good description of all the large-p_T data up to and including ISR energies. For a review, see reference 11. However, data from the much higher energy of the CERN $\bar{p}p$ Collider seem to come much nearer to being scale-free: see the lecture by Dowell.

Most of the theoretical analysis of large-p_T processes has been in the framework of hard-scattering models, figure 27. In the middle of this

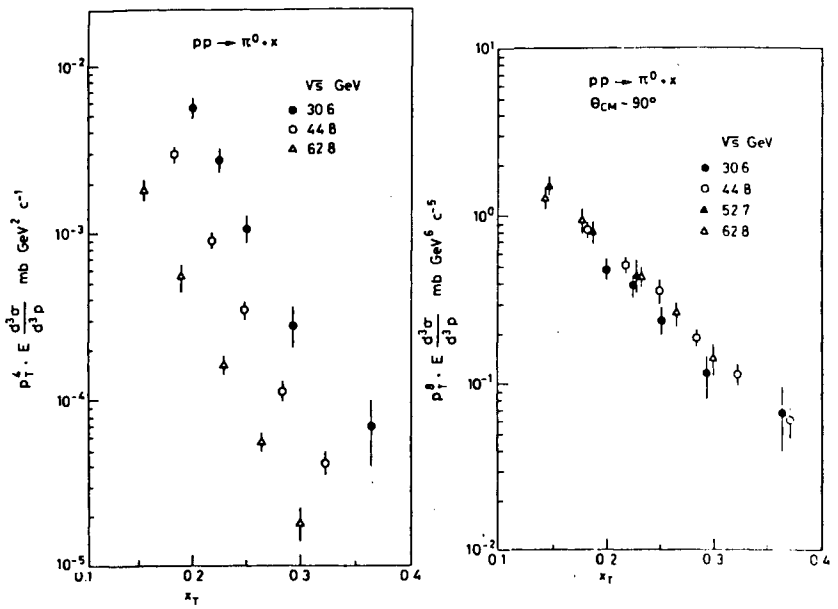

Figure 26 : $p_T^4 Ed\sigma/d^3p$ and $p_T^8 Ed\sigma/d^3p$ for $pp \to \pi^0 X$ at 90^0 (CCOR collaboration).

diagram there is a wide-angle scattering A+B → C+D. The question, which is not answered so far as the ISR and lower-energy data are concerned, is what are A,B,C and D. In QCD they would be quarks and gluons and the central wide-angle scattering would be calculated from perturbative QCD (see §4). In lowest order, before scale-breaking effects are introduced, one obtains n = 4, but higher-order corrections increase the value of n. There are various uncertainties in the calculation, partly because one does not know the distribution of gluons in the initial hadrons very well, partly because one again has to try and take account of the intrinsic transverse momentum of the partons, and partly because of the usual problems with higher-order QCD corrections that I discuss in §5; in particular there is a K-factor, whose value is not yet known. I estimate

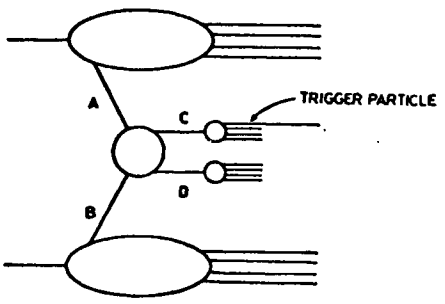

Figure 27 : Hard-scattering models.

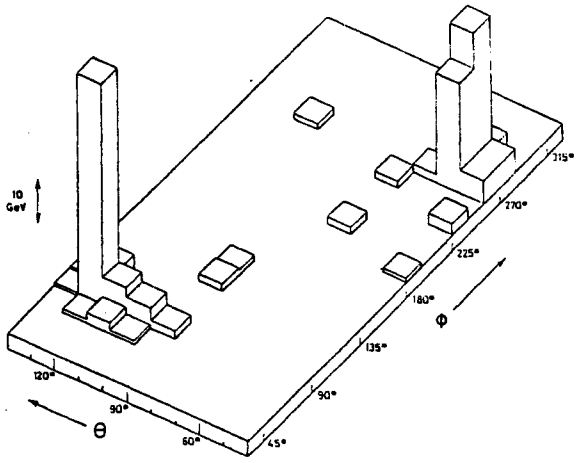

Figure 28 : Evidence for jets at the $\bar{p}p$ Collider (UA2).

that the uncertainty is at the one-order-of-magnitude level!

In figure 27, the objects C and D that emerge from the wide-angle scattering are shown as materialising as jets of hadrons. Certainly one expects this if C and D are quarks or gluons. One of the particles in the jet C is indicated as being the "trigger particle", that is it is the detected pion in (45). The ISR data of several years ago already confirm [11] the presence of two transverse jets in large-p_T events. Figure 28 shows some very beautiful new evidence from the $\bar{p}p$ Collider. What is drawn is a map of a calorimeter that surrounds the collision region; θ and ϕ are the polar and azimuthal angles. The calorimeter is divided into cells, and the "vertical" scale measures the energy deposited in the cells. Two transverse jets, which emerge back-to-back at $\theta = 60^{\circ}$ and $\theta = 120^{\circ}$, are clearly seen.

4. A QCD CALCULATION

To give some practice with QCD perturbation theory, I now calculate

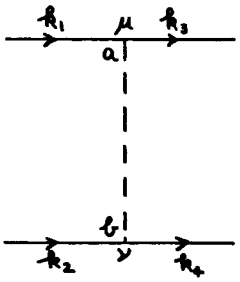

Figure 29 : Lowest-order graph for the wide-angle scattering ud → ud.

the central wide-angle scattering in figure 27, for the case where A,B,C and D are all quarks. For simplicity I choose two quarks of different flavours, u and d say, so that in lowest order of QCD perturbation theory there is only one Feynman graph, figure 29.

The usual procedure, which may or may not be valid, is to ignore the fact that the initial quarks A,B in figure 27 are constituents of their parent hadrons and therefore "off shell". One calculates the differential cross-section $d\sigma/dt$ for the central scattering with all the quark lines "on-shell", and then convolutes it with the appropriate quark density functions $q(x)$ for the initial hadrons (see (12)).

It is usual to use the variables

$$s = (k_1+k_2)^2 \ , \quad t = (k_1-k_3)^2 \ , \quad u = (k_1-k_4)^2 \tag{49}$$

Only two of these are independent: their sum is the sum of the squared masses of the four quarks in figure 29. If there were no complications from spin and colour, at large s the differential cross-section would be given[12] in terms of the matrix element M by

$$\frac{d\sigma}{dt} = \frac{1}{16\pi s^2} |M|^2 \tag{50}$$

In our calculation, $|M|^2$ must be summed over the possible spin and colour states of the final quarks, and averaged over their possible initial spin and colour states.

The Feynman rules for QCD are given by Taylor in his lectures. They yield

$$M = \tfrac{1}{2}\left[\bar{u}_3(-ig\gamma^\mu T_a)u_1\right] \cdot \frac{i\delta_{ab}g_{\mu\nu}}{t} \cdot \left[\bar{u}_4(-igT^\nu T_b)u_2\right] \tag{51}$$

Here I have followed a convention that is frequently used: for $(SU3)_{colour}$ one writes T in place of the Gell-Mann matrix ($\frac{1}{2}\lambda$), which is reserved for $(SU3)_{flavour}$. Thus T is a 3×3 matrix whose rows and columns correspond to quark colours. I have used a shorthand for the spinors in (51), for example u_1 stands for $u(k_1;s_1,c_1)$, where s_1 is a spin label and c_1 is a colour label. The two factors in square brackets in (51) arise from the two quark lines; in between them I have written the gluon propagator.

From (51) it follows straightforwardly that

$$M = \frac{g^2}{t}\left[\bar{u}_3\gamma^\mu T_a u_1\right]\left[\bar{u}_4\gamma_\mu T_a u_2\right] \tag{52}$$

Each initial quark has two possible spin states and two possible colour states, so we need

$$(\tfrac{1}{2})^2\ (\tfrac{1}{3})^2 \sum_{\substack{s_1\ldots s_4\\ c_1\ldots c_4}} M\,M^* \tag{53}$$

When we calculate M^* we need to remember that we have to introduce a different set of dummy indices of summation, for example μ' and a', in place of μ and a.

Spin sums such as that in (53) are a standard exercise in QED, and are carried out by taking traces of Dirac γ matrices[12]. The colour sum gives a further trace over T-matrices, which arises because of the completeness relation

$$\sum_{s,c} u(k;s,c)\ \bar{u}(k;s,c) = (\gamma k+m)\ I \tag{54}$$

with I the unit 3×3 matrix is in colour space. One finds that

$$\sum_{\substack{s_1 s_3\\ c_1 c_3}} \left[\bar{u}_3\gamma^{\mu}T_a u_1\right]\ \left[\bar{u}_3\gamma^{\mu'}T_{a'}u_1\right]^*$$

$$= \{\mathrm{Tr}(\gamma.k_3+m)\gamma^{\mu}(\gamma.k_1+m)\gamma^{\nu}\}\{\mathrm{Tr}\ T_a T_{a'}\}$$

$$= 4\left[k_3^{\mu}k_1^{\mu'} + k_1^{\mu}k_3^{\mu'} + (m^2 - k_1.k_3)g^{\mu\mu'}\right]\{\tfrac{1}{2}\delta_{aa'}\} \tag{55}$$

To calculate (53), (55) has to be multiplied by a similar expression involving k_2 and k_4. One then uses

$$\begin{aligned} g^{\mu\mu'}g_{\mu\mu'} &= g^{\mu}_{\mu} = 4\\ \delta_{aa'}\delta_{aa'} &= \delta_{aa} = 8 \end{aligned} \tag{56}$$

This gives

$$\tfrac{1}{4}\cdot\tfrac{1}{9}\ \Sigma\, M\,M^* = \tfrac{4}{9}g^4\ \frac{s^2+u^2}{t^2} \tag{57}$$

where I have neglected m^2 compared with the large variables s and u.

Inserting $g^2/4\pi = \alpha_s$, we have finally

$$\frac{d\sigma}{dt} = \tfrac{4}{9}\pi\alpha_s^2\ \frac{s^2+u^2}{t^2} \tag{58}$$

We now have a big problem. The coupling α_s is a running coupling, so what should we choose as its argument? At the present time, we do not know how to give a straightforward answer to this question. It involves

calculating higher-order corrections to figure 29 and the problem of renormalisation, which I now discuss.

5. HIGHER ORDER TERMS

Simple Example of Renormalisation

Quantum field theories are plagued with infinities (see Taylor's lectures). In some cases, these infinities can be explained away, and then the field theory is said to be renormalisable. QCD holds the unique position that it is the only renormalisable field theory that is a plausible candidate for describing the strong interactions.

To get a simple idea of the spirit of renormalisation, consider the classical theory of a free electron at rest at the origin. Because the electron is charged, there is an electric field

$$\mathcal{E} = \frac{-e}{4\pi\varepsilon_o r^2} \tag{59}$$

with which is associated the Coulomb energy

$$E_{Coulomb} = \int d^3\underset{\sim}{r}\ \tfrac{1}{2}\varepsilon_o \mathcal{E}^2 = \frac{e^2}{8\pi\varepsilon_o}\int \frac{dr}{r^2} \tag{60}$$

So the total energy is

$$E = m_o c^2 + E_{Coulomb} \tag{61}$$

where m_o is the electron's mechanical mass (whatever that may mean). But the total energy of an electron at rest may also be written as $E = mc^2$, where m is the mass value in the particle data tables. So

$$m = m_o + c^{-2} E_{Coulomb} \tag{62}$$

For a pointlike electron, the integration in (60) extends down to r = 0 and so $E_{Coulomb}$ is infinite. But this does not matter, because the only quantity in (62) that is measurable is m. Here, renormalisation means including the infinite quantity $c^{-2}E_{Coulomb}$ along with the unmeasurable "bare" mass m_o, to give the finite, measured mass m.

Renormalisation in QED

In quantum field theory, the idea behind renormalisation is similarly to re-arrange the perturbation expansion, so that infinite quantities are included along with unmeasurable ones, so as to give finite measurable quantities. It is worth observing that the renormalisation would have to be done even if there were no infinities, and it is lucky that the renormalisation also eliminates the infinities (or, maybe, it is an

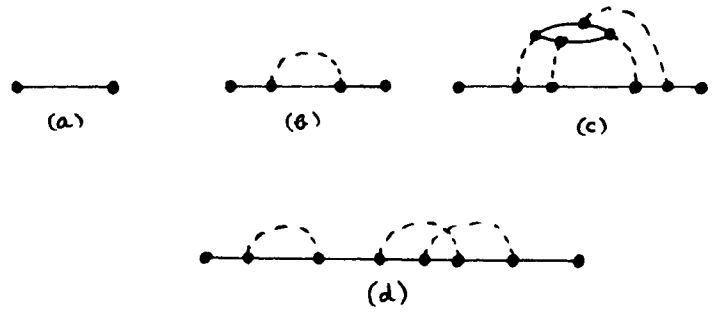

Figure 30 : The bare electron propagator, with simple examples of self-energy insertions.

indication that we have the right theory!).

For simplicity, pretend that the electron has no spin. Then any internal electron line in a Feynman graph corresponds to a propagator

$$S_o(p^2) = \frac{1}{p^2-m_o^2} \tag{63}$$

Here p is the momentum on the line and m_o is the mass that is originally put in the Lagrangian. It is not the physical mass, because it does not include the electromagnetic part.

Now for any Feynman graph in which two adjacent vertices are simply connected by an electron line, there is an infinity of more complicated graphs where so-called "self-energy" insertions are made in that line. Examples are shown in figure 30, where (a) is a pair of vertices connected by the "bare" propagator $S_o(p^2)$ and the rest of the graph is not shown. Of the three examples of insertions, (d) differs from (b) and (c) in that it is "one-particle reducible": it may be divided into two separate parts by cutting just one line. Suppose that we call Σ the sum of all one-particle-irreducible insertions; because of Lorentz invariance, it is a function of p^2. Then we can write the sum of all insertions, both irreducible and reducible, together with the original bare propagator, in the form indicated in figure 31. Written as an equation, figure 31 is

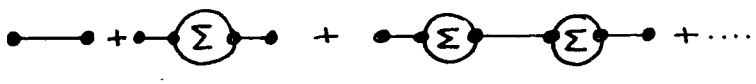

Figure 31 : The dressed electron propagator, where Σ is the sum of all one-particle-irreducible self-energy insertions.

$$S(p^2) = S_o(p^2) + S_o(p^2)\Sigma(p^2)S_o(p^2) + S_o\Sigma S_o\Sigma S_o + ... \quad (64)$$

So we may take account of all self-energy insertions by using only Feynman graphs where there are no such insertions, but replacing the bare propagator S_o by the "dressed" propagator $S(p^2)$.

The infinite series (64) may easily be summed:

$$S(p^2) = \frac{S_o(p^2)}{1 - S_o(p^2)\Sigma(p^2)} = \frac{1}{S_o^{-1}(p^2) - \Sigma(p^2)}$$

$$= \frac{1}{p^2 - m_o^2 - \Sigma(p^2)} \quad (65)$$

Now make a Taylor expansion of $\Sigma(p^2)$ about some point $p^2 = m^2$, which remains to be chosen:

$$\Sigma(p^2) = \Sigma(m^2) + (p^2-m^2)\Sigma'(m^2) + \tfrac{1}{2}(p^2-m^2)\Sigma''(m^2) + ... \quad (66)$$

or, equivalently,

$$\Sigma(p^2) = A + (p^2-m^2)B + (p^2-m^2)\tilde{\Sigma}(p^2) \quad (67)$$

where A and B are constants and the function $\tilde{\Sigma}$ has the property

$$\tilde{\Sigma}(m^2) = 0 \quad (68)$$

It turns out that in QED, A and B are infinite but $\tilde{\Sigma}$ is a finite function.

Inserting (67) into (65) gives

$$S(p^2) = \frac{1}{p^2 - m_o^2 - A - (p^2-m^2)B - (p^2-m^2)\tilde{\Sigma}(p^2)} \quad (69)$$

We now choose the value of m^2 to be

$$m^2 = m_o^2 + A \quad (70)$$

so that

$$S(p^2) = \frac{1}{(p^2-m^2)(1-B-\tilde{\Sigma}(p^2))} \quad (71)$$

The bare propagator (63) has a singularity at $p^2 = m_o^2$. The electromagnetic self-energy corrections shift this to give a singularity at $p^2 = m^2$ in the dressed propagator (71). The unmeasurable quantities m_o^2 and A have now disappeared from the formalism; only the physical mass m^2,

given by (70), remains. This is called mass renormalisation: the perturbation expansion has been rearranged in such a way that the infinite constant A has gone.

However, the infinite constant B still remains. It is removed by a charge renormalisation, which is another rearrangement of the perturbation expansion. One removes from the dressed propagator (71) the factor

$$Z_2 = \frac{1}{1-B} \tag{72}$$

so that it becomes

$$S(p^2) = \frac{1}{(p^2-m^2)(1-Z_2\tilde{\Sigma}(p^2))} \tag{73}$$

So as not to change the numerical value of the Feynman graph in which $S(p^2)$ is being used, a factor $\sqrt{Z_2}$ is instead included with the charge on the vertices at either end of the internal electron line that corresponds to $S(p^2)$. Since all internal vertices have two electron lines (and one photon line) attached to them, this implies the change

$$e_o \to e_1 = (\sqrt{Z_2})^2 e_o \tag{74}$$

where e_o is the original charge that was put in the Lagrangian.

This simultaneous change of charge and electron propagator leaves unchanged graphs in which every vertex has two electron propagators attached to it. Graphs that have electrons as external lines need special treatment, called wave function renormalisation. The graphs that are used to calculate $\tilde{\Sigma}(p^2)$ are insertions in a propagator, and so their left-most and right-most vertices only have one electron propagator. The $\tilde{\Sigma}(p^2)$ in (73) was supposed to be calculated using $S_o(p^2)$ and e_o; if instead it is calculated with $S(p^2)$ and $Z_2 e_o$ it changes by a factor Z_2. So if we use the new prescription to calculate $\tilde{\Sigma}$, (73) becomes

$$S(p^2) = \frac{1}{(p^2-m^2)(1-\tilde{\Sigma}(p^2)} \tag{74}$$

which no longer contains any infinite quantity.

The photon propagator is dealt with in a similar way, though with one important difference: no mass renormalisation is needed. This feature may be shown to result from the gauge invariance. So the photon propagator contributes another charge renormalisation: (74) becomes

$$e_o \to e_2 = Z_2\sqrt{Z_3}\, e_o \tag{75}$$

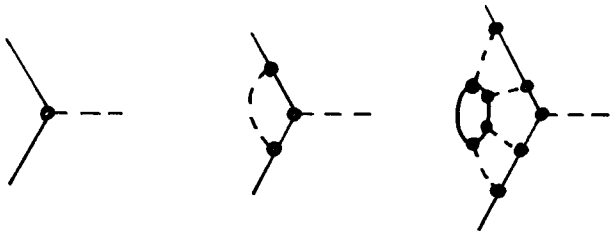

Figure 32 : The bare vertex and vertex insertions.

There is only one power of $\sqrt{Z_3}$, because each vertex has only one line attached to it. The renormalised, dressed photon propagator is

$$D(k^2) = \frac{1}{k^2(1-\tilde{\pi}(k^2)} \tag{76}$$

where

$$\tilde{\pi}(o) = 0 \tag{77}$$

Finally, there is a charge renormalisation from vertex insertions. For every graph where there is a bare vertex, the first term in figure 32, there is an infinity of other graphs in which various insertions are made in that vertex, such as those drawn in the figure. In the spinless model, Lorentz invariance implies that these insertions are functions of the squared momenta p^2, p'^2 of the two electron legs, and the squared momentum k^2 of the photon. Thus the contribution e_2 from the bare vertex now becomes an expression of the form

$$e_2(1 + \Gamma(p^2, p'^2, k^2)) \tag{78}$$

where Γ represents the sum of all the vertex insertions. Define

$$L = \Gamma(m^2, m^2, 0) \tag{79}$$

so that (78) becomes

$$e_2(1 + L + \tilde{\Gamma}(p^2, p'^2, k^2)) \tag{80}$$

where

$$\tilde{\Gamma}(m^2, m^2, 0) = 0 \tag{81}$$

The constant L is infinite, so we extract a factor

$$Z_1^{-1} = 1 + L \tag{82}$$

from inside the bracket in (80) and instead include it in the charge. So the charge becomes

$$e = Z_1^{-1} e_2 = Z_1^{-1} Z_2 Z_3^{\frac{1}{2}} e_o \tag{83}$$

and instead of (80) we have

$$e(1 + Z_1 \tilde{\Gamma}(p^2, p'^2, k^2) \tag{84}$$

This rearrangement leaves all diagrams unchanged. However, if we calculate $\tilde{\Gamma}$ with the new prescription, it changes by a factor Z_1^{-1}, because it is not calculated from complete diagrams: it represents the sum of vertex insertions with the charge factored out. So if we use the new prescription to calculate $\tilde{\Gamma}$, we have instead of (84)

$$e(1 + \tilde{\Gamma}(p^2, p'^2, k^2)) \tag{85}$$

and the infinity has now gone away; it has been fully absorbed in the charge.

Summary of QED Renormalisation

The conclusion is that one should calculate only graphs without propagator and vertex insertions, and used the dressed propagators

$$\begin{aligned} S(p) &= \frac{1}{(\gamma.p - m)(1 - \tilde{\Sigma}(p))} \\ D^{\mu\nu}(k) &= \frac{-g^{\mu\nu} + \frac{k^\mu k^\nu}{k^2}}{k^2(1 - \tilde{\pi}(k^2))} \end{aligned} \tag{86}$$

for the electron and photon respectively. I have here stated the propagators taking proper account of the spins of the particles, and I have used the Landau gauge because it is simplest for discussing renormalisation. At each vertex one uses

$$e(\gamma^\mu + \tilde{\Gamma}^\mu(p, p', k)) \tag{87}$$

where $\tilde{\Gamma}$ is now a 4×4 matrix in Dirac space. Constraints analogous to (68), (77) and (81) are imposed at $\gamma.p = \gamma.p' = m$, $k^2 = 0$, so that near this point the propagators and the vertex revert to the forms that the bare propagators and vertex took before the renormalisation, though with charge e and mass m instead of the original e_o and m_o. e and m are

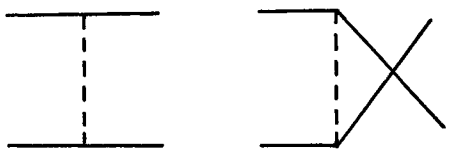

Figure 33 : ee scattering in lowest order.

identified as the mass and charge that are listed in the particle data tables. To show this, one calculates, for example, low-energy small-t electron-electron scattering to lowest order in α using the graphs of figure 33 and finds that they correctly give the usual Mott formula. In particular, the graphs give the static Coulomb force.

Renormalisation in QCD

Because no free quarks have been observed, their mass and "chromo-Coulomb" coupling g are not listed in the data tables. So the renormalisation procedure that I have described cannot be exactly followed in QCD. In fact there is considerable freedom as to the choice of renormalisation scheme. It is worth stressing that the same freedom exists also in QED, if one chooses to use it, though there one more usually chooses to introduce the static charge and mass in the way I have described. The different renormalisation schemes must all lead to the same physical outputs, a fact that is used to derive a powerful act of equations called renormalisation group equations[13].

Of the many possibilities, three schemes are commonly found in the QCD literature[14]. These are:

MS (minimal subtaction)
$\overline{\text{MS}}$ (modified minimal subtaction)
MOM (momentum subtraction)

Of these, MS and $\overline{\text{MS}}$ are mathematically the simplest, but MOM is closer to the procedure that I described for QED and many people think that it is better motivated physically.

Whatever scheme is chosen it is useful to introduce a regularisation procedure to help in handling the infinities. A very convenient one is dimensional regularisation because, as Taylor describes in his lectures, this manifestly preserves the gauge invariance. One works in a number of space-time dimensions d different from 4, and calculates quantities as functions of

$$\varepsilon = \tfrac{1}{2}(d-4) \qquad (88)$$

One finds $1/\varepsilon$ singularities, which are absorbed away by the renormalisation procedure, so leaving a finite result when $\varepsilon \to 0$ at the end of the

calculation.

Before renormalisation, the dressed gluon propagator is found[14] to take the form (neglecting spin again)

$$D(k^2) = \frac{1}{k^2\left[1-N(\frac{1}{\epsilon}+\gamma-\log 4\pi)-\pi_1(k^2)\right]} \tag{89}$$

where γ is Euler's constant ($\gamma = 0.577\ldots.$) and π_1 is a function that has no $1/\epsilon$ singularities. N is some constant. I could have absorbed the $(\gamma-\log 4\pi)$ term in $\pi_1(k^2)$, but I have displayed it explicitly because here, and also in the quark propagator and the vertex functions, it appears with the same coefficient as does $1/\epsilon$. The renormalisation extracts a factor Z_3 from $D(k^2)$ and instead includes it in the coupling. This factor must include the $1/\epsilon$ singularity, in order that the propagator remains finite when $\epsilon \to 0$ after the renormalisation. In MS, one defines simply

$$Z_3^{-1} = 1 - N/\epsilon \tag{90}$$

In $\overline{\text{MS}}$, one recognises that the $1/\epsilon$ is everywhere accompanied by $(\gamma-\log 4\pi)$, and so defines

$$Z_3^{-1} = 1-N(\frac{1}{\epsilon}+\gamma-\log 4\pi) \tag{91}$$

In MOM one includes also a part of the function π_1 in Z_3 :

$$Z_3^{-1} = 1-N(\frac{1}{\epsilon}+\gamma-\log 4\pi) - \pi_1(\mu^2) \tag{92}$$

In the MOM scheme, the renormalisation is arranged so that the quark and gluon propagators, and their vertex function, reverts to the form that the corresponding bare functions took before the renormalisation, near the arbitrarily-chosen point $p^2 = p'^2 = k^2 = \mu^2$. The mass μ is called the renormalisation scale. As Taylor describes, one also introduces a mass μ in the relation between the bare and renormalised couplings so as to keep the latter dimensionless when $\epsilon \neq 0$. That is

$$g = Z_1^{-1}Z_2Z_3^{\frac{1}{2}}g_o\,\mu^{\epsilon} \tag{93}$$

Compare (83). It is convenient to choose the same μ in (93) as in (92). Introducing μ through (93) also defines the renormalisation scale in MS and $\overline{\text{MS}}$.

The value of g depends, for given g_o, on the value chosen for μ. This is both because of the explicit appearance of μ in (93), and because the renormalisation constants Z vary with μ. This is why one calls g a

"running" coupling. One writes

$$\frac{g^2}{4\pi} = \alpha_s(\mu^2) \tag{94}$$

In any scheme, one-loop calculations give

$$\alpha_s(\mu^2) = \frac{12\pi}{(33-2N_f)\log Q^2/\Lambda^2} \tag{95}$$

where N_f is the number of quark flavours and Λ is a constant. See Taylor's lectures. The value of Λ cannot be calculated: it must be taken from experiment. It takes different values in different renormalisation schemes. It may be shown[14] that

$$\begin{aligned} \Lambda_{\overline{MS}} &\approx 3\Lambda_{MS} \\ \Lambda_{MOM} &\approx 2\Lambda_{\overline{MS}} \end{aligned} \tag{96}$$

Consider two different schemes, with couplings $\alpha_1(\mu^2)$ and $\alpha_2(\mu^2)$. Then

$$\alpha_1(\mu^2) = \frac{\beta_o}{\log\mu^2/\Lambda_1^2} \qquad \alpha_2(\mu^2) = \frac{\beta_o}{\log\mu^2/\Lambda_2^2}$$

$$\beta_o = \frac{12\pi}{33-2N_f} \tag{97}$$

For $\mu >> \Lambda_1, \Lambda_2$ we may expand α_2 in powers of α_1 :

$$\alpha_2(\mu^2) = \frac{\beta_o}{\log\frac{\mu^2}{\Lambda_1^2} - \log\frac{\Lambda_2^2}{\Lambda_1^2}}$$

$$= \frac{\beta_o}{\log\frac{\mu^2}{\Lambda_1^2}}\left(1 + \frac{\log\Lambda_2^2/\Lambda_1^2}{\log\mu^2/\Lambda_1^2} + \ldots\right)$$

$$= \alpha_1(\mu^2)\left[1 + \frac{\log\Lambda_2^2/\Lambda_1^2}{\beta_o}\alpha_1(\mu^2) + \ldots\right] \tag{98}$$

So a change of renormalisation scheme has the effect

$$\alpha_s \rightarrow \alpha_s \left[1 + A \frac{\alpha_s}{\pi} + \ldots.\right] \tag{99}$$

where A is a constant. It is straightforward to see from (95) that changing the renormalisation scale has a similar effect.

Suppose now that some physical quantity P has been calculated in some scheme with a given choice of renormalisation scale, giving the result

$$P = B\,\alpha_s^N \left[1 + C \frac{\alpha_s}{\pi} + \ldots.\right] \tag{100}$$

where B and C are constants or functions of the variables in the problem. If we change either the scheme or the scale, (99) gives

$$P \rightarrow B\,\alpha_s^N \left[1 + (C + NA) \frac{\alpha_s}{\pi} + \ldots.\right] \tag{101}$$

The statement that the theory is renormalisable implies that the sums of the infinite series (100) and (101) are equal. However, in practice one does not calculate the full infinite series; one truncates it after just a few terms, maybe even after the first term. The truncated series are not numerically equal.

When one truncates the series, throwing away an infinite number of terms after the first few, one implicitly assumes that this introduces only a small error. The question then arises: in what scheme, and for what value of the renormalisation scale, is this a good approximation? Because one has not calculated the terms that have been discarded, this question cannot be answered, except by guesswork.

Often, one just compares the first term with experiment, $P = B\alpha_s^N$. One is then implicitly assuming a renormalisation scheme that makes the rest of the series negligible. One cannot identify this scheme, beyond saying that it is the one appropriate for a leading-order calculation of the quantity P. The comparison with experiment yields a corresponding Λ, $\Lambda_{L.O.(P)}$ say. If one now goes through the same procedure for some other physical quantity P', the result will be another Λ, $\Lambda_{L.O.(P')}$. There is no reason to expect that $\Lambda_{L.O.(P)} = \Lambda_{L.O.(P')}$.

If two terms are calculated in P,

$$P = B\alpha_s^N \left(1 + C \frac{\alpha_s}{\pi}\right) \tag{102}$$

it is often assumed that it is valid to compare this with experiment if $|C| \ll 1$. This is based on the hope that the other terms, not calculated, will then also have small coefficients. But, because the other terms have not been calculated, this cannot be more than a hope. Calculations find that usually, with a sensible choice of μ, the MS scheme leads to a large

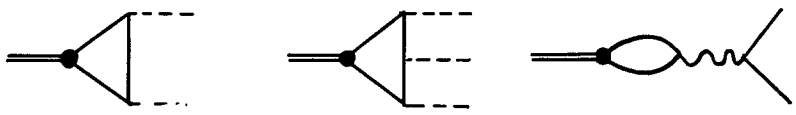

Figure 34 : Decays of $b\bar{b}$ states: (a) $\eta_B \to gg$ or $\gamma\gamma$ (b) $\Upsilon \to ggg$ (c) $\Upsilon \to e^+e^-$

value of C, $\overline{MS}$ a rather smaller value, and MOM a smaller value still. However, this statement must be treated with caution.

Examples of nonleading terms

In a meson composed of heavy quarks, one expects the quarks to be close together. Compare the Bohr radius of the hydrogen atom, which is inversely proportional to the reduced mass. So one might expect the decay of the meson to be a short-distance reaction, describable by perturbative QCD.

As an example, consider the decay of η_B, the pseudoscalar $b\bar{b}$ state. If QCD perturbation theory is valid, its hadronic decay is described by figure 34a, where $\eta_B \to gg$. As usual, it is supposed that the gluons subsequently hadronise so as to form two jets. At the left-hand vertex there is the η_B wave function. In order to eliminate this, one may compare the gg decay with $\eta_B \to \gamma\gamma$, which is calculated from the same diagram but with the gluons replaced by photons. The result is[15]

$$\frac{\Gamma(\eta_B \to gg)}{\Gamma(\eta_B \to \gamma\gamma)} = B\,\alpha_s^2 \left[1 + C\,\frac{\alpha_s}{\pi} + \ldots.\right] \qquad (103)$$

where, with renormalisation scale $\mu = M_{\eta_B}$,

$$\begin{aligned} C &= 22 \quad (MS) \\ C &= 14 \quad (\overline{MS}) \\ C &= 8 \quad (MOM) \end{aligned} \qquad (104)$$

So, even in MOM, the second term in (103) is so large that one cannot confidently hope that the uncalculated terms are negligible. However, physical intuition suggests a way to improve things. The coupling α_s enters in figure 34a at the two gluon vertices. The gluons share the momentum of the η_B; on average they each take half of it. So maybe it is more sensible to take $\mu = \frac{1}{2}M_{\eta_B}$. Then, in MOM, C = 2, which seems good.

However, the hope that a little physical intuition shows the right procedure is not sustained by the calculation from figure 34b of the 3-gluon decay of the Υ. The procedure that improved things for $\eta_B \to gg$

actually here make things worse. In order again to eliminate the Υ wave function, compare the decay $\Upsilon \to ggg$ with the decay $\Upsilon \to e^+e^-$, calculated from figure 34c. The result is[16]

$$\frac{\Gamma(\Upsilon \to ggg)}{\Gamma(\Upsilon \to e^+e^-)} = B\,\alpha_s^3 \left[1 + C\,\frac{\alpha_s}{\pi} + \ldots.\right] \qquad (105)$$

With renormalisation scale $\mu = M_\Upsilon$, the value of C in $\overline{MS}$ is 9, while in MOM it is -1. So in MOM things already look good. However, as above, one might now try replacing $\mu = M_\Upsilon$ by $\mu = M_\Upsilon/n$, where n is the number of gluons; here n = 3. Then in $\overline{MOM}$ C = -14. So this is not a good thing to do here.

Another example[7,17] that has caused some anguish is the cross-section for the production of 3 jets in e^+e^- annihilation. Until recently, all four PETRA experiments agreed that if one fits the data to a leading order calculation, the result is $\alpha_s(\sqrt{s} = 30\ \text{GeV}) \approx 0.18$, corresponding to $\Lambda_{\text{L.O(3 jets)}} \approx 250$ MeV. (As I mentioned in §3, more recently it has been suggested that this result may be sensitive to the jet hadronisation model used to analyse the data.) Calculations of the next-to-leading order correction to the 3-jet cross-section give different answers. Some authors find that it is large in $\overline{MS}$, so that if the two-term formula were compared with the data $\Lambda_{\overline{MS}}$ would be found to be only about 40 MeV. The opposing view is that it is small in $\overline{MS}$, leading to $\Lambda_{\overline{MS}} \approx 500$ MeV. The resolution of the controversy seems to be that the calculated cross section is sensitive to just how one separates 3-jet events from 2-jet events. In §3 I pointed out that figure 17 yields events that are sometimes 2-jet and sometimes 3-jet, and the hadronisation of the quarks and the gluon makes it difficult to define a clean separation between the two.

6. CONCLUSIONS

The presence of higher twists that cannot be calculated, and problems with the scheme dependence and the slow convergence of the QCD perturbation expansion in powers of α_s, imply that accurate calculation is not yet possible. Nevertheless, many things are explained qualitatively by QCD. While in each case it may be possible to find an alternative explanation, if one considers everything together it is hard to believe that QCD is not at work.

I suspect that further progress requires more calculations, and more data to compare them with. One may hope that in this way one may learn how to overcome the difficulties. I suspect that pure thought is not enough: the data must point the right way. So more work is needed, by both theorists and experimentalists.

REFERENCES

1. F.E. Close, Introduction to Quarks and Partons, (Academic Press, London 1979).

2. P.V. Landshoff and J.C. Polkinghorne, Physics Reports 5C, (1972).

3. F. Eisele, report to the XXI International Conference on High Energy Physics, Paris 1982.

4. C.E. DeTar, S.D. Ellis and P.V. Landshoff, Nuclear Physics B87, 176 (1975); G.T. Bodwin, S.J. Brodsky and G.P. Lepage, Phys. Rev. Lett. 47, 1799 (1981); W.A. Lindsay, D.A. Ross and C.T. Sachrajda, Southampton preprint SHEP 81/82-6; P.V. Landshoff and W.J. Stirling, Z. Physik C14, 251 (1982).

5. Photon-Photon Interactions, ed. G.W. London (World Scientific, Singapore 1981).

6. P.V. Landshoff, report to International Conference on High Energy Physics, Lisbon 1981 (Cambridge preprint DAMTP 81/22); D.H. Perkins, Proc. 1981 CERN-JINR School of Physics (CERN 82-04).

7. G. Wolf, report to XXI International Conference on High Energy Physics, Paris 1982.

8. G. Altarelli, Physics Reports 81, 1 (1982).

9. F. Halzen and D.M. Scott, 1981 Moriond Workshop on Lepton Pair Production (Madison preprint DOE/ER/00881-199 or Cambridge preprint DAMTP 81/7).

10. G. Altarelli, R.K. Ellis and G. Martinelli, Nuclear Physics, B143, 521 (1978); F. Khalafi, Z. Physik C14, 135 (1982); P.V. Landshoff and W.J. Stirling, reference 4.

11. M. Jacob and P.V. Landshoff, Physics Reports 48, 285 (1978); D.I. Sivers, S.J. Brodsky and R. Blankenbecler, Physics Reports 23, 1 (1976).

12. I.J.R. Aitchison and A.J.G. Hey, Gauge Theories in Particle Physics, (Adam Hilger, Bristol 1982).

13. E. Leader and E. Predazzi, Gauge Theories and the New Physics, (Cambridge University Press 1982).

14. W. Marciano and H. Pagels, Physics Reports 36, 137 (1978); W. Celmaster and R.J. Gonsalves, Phys. Rev. D20, 1420 (1979).

15. R. Barbieri, G. Curci, E. d'Emilio and E. Remiddi, Nuclear Physics B154, 535 (1979).

16. P.B. McKenzie and G.P. Lepage, Phys. Rev. Lett. 47, 1244 (1981).

17. P.V. Landshoff, reference 6.